Seismic Attenuation Analysis of Búzios oil field via Viscoelastic Modelling

Fabrício Augusto[1]*, Danielle Tostes[1], Marco Cetale[1], Roger Moreira[1], Djalma Soares[2], Felipe Costa[1] and Felipe Capuzzo[1]

[1]UFF/DOT/GISIS, [2] PETROBRAS/CENPES

Abstract

Absorption and dispersion in seismic waves affect the amplitude and phase of the seismic data. The viscoelastic models take into account such effects and can help the understanding of the attenuation that they cause. The poststack seismic data of the Búzios field was compared to a viscoelastic modelling to study the attenuation in the real data. The comparison between the amplitude spectra from three selected regions in seismic data and the synthetic data generated with a layered model using different attenuation settings indicated that the shallower sediment is more dissipative (lower Q values) than the deepest ones.

Introduction

The effects of absorption and dispersion in seismic waves cause attenuation of the amplitude and deform the waveform. These effects can compromise the quality of the seismic data and decrease the resolution of the seismic imaging. The heterogeneities and anelastic properties of the medium contribute to the seismic wave energy dissipation (Wang, 2008), resulting in seismic attenuation.

The viscoelastic mechanical models are an usual way to describe anelastic media taking into account attenuation and waveform distortion effects. The standard linear solid (SLS), also known as Zener model (Zener, 1948), was proposed by Poynting and Thomson (1903) and reviewed by several authors (Findley et al., 1989; Carcione, 2015; Schuster, 2017). It gives a more realistic representation of material media, such as rocks, polymers and metals (Carcione, 2015).

Robertsson et al. (1994) developed a conditionally stable finite-difference scheme for viscoelastic wave simulation. This scheme allows to propagate attenuated waveform for different quality factor Q models and heterogeneous media. Fan et al. (2016) improved the expressions separating the memory variables of P and S waves based on the method of Robertsson et al. (1994) and implemented 2-D viscoelastic finite-difference modeling.

The main goal of this work is to investigate the characteristics of seismic attenuation present at Buzios field, using real data and viscoelastic wave equation modelling. The impact of quality factor Q in the seismic modelling is also analysed.

Methodology

Viscoelasticity

In the viscoelastic hypothesis, the current value of the stress tensor (σ_{ij}) depends upon the complete past history of the components of the stress tensor (ε_{kl}) (Christensen, 1982). It can be expressed by the constitutive relation:

$$\sigma_{ij} = \psi_{ijkl} * \dot{\varepsilon}_{kl} = \dot{\psi}_{ijkl} * \varepsilon_{kl} \qquad (1)$$

where ψ_{ijkl} corresponds to the relaxation function, $*$ represents a convolution and the dot indicates a temporal derivative.

The *Standard Linear Solid* (SLS) was chosen to describe the viscoelastic behavior of materials. The SLS model is a combination series of a spring and a Kelvin-Voigt model, which consists of a spring and a dashpot connected in parallel (see Figure 1).
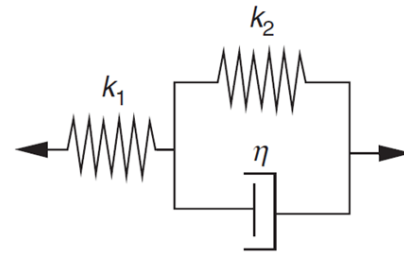

Figure 1: Mechanical model for Standard Linear Solid.

The relaxation function determines the behavior of the material and for SLS is given by:

$$\psi(t) = M_R \left[1 - \left(1 - \frac{\tau_\varepsilon}{\tau_\sigma} e^{-t/\tau_\sigma} \right) \right] H(t), \qquad (2)$$

where M_R is the relaxation modulus of the medium and $H(t)$ is the heaviside function (Blanch et al., 1993). τ_σ and τ_ε correspond to the relaxation times.

The effects of absorption and dispersion can be quantified using the quality factor Q, which for the Zener model can be written in terms of the relaxation times τ_σ and τ_ε:

$$Q(\omega) = \frac{1 + \omega^2 \tau_\varepsilon \tau_\sigma}{\omega(\tau_\varepsilon - \tau_\sigma)}. \qquad (3)$$

The first order system of differential equation for solving the viscoelastic wave equation is given by Robertsson et al. (1994):

$$\begin{cases} \partial_j \sigma_{ij} - \rho \partial_t v_i = -\rho f_i \\ \dot{\sigma}_{ij} = \dot{\Lambda} * \delta_{ij} \dot{\varepsilon}_{kk} + 2\dot{M} * \dot{\varepsilon}_{ij}. \end{cases} \qquad (4)$$

Defining

$$\Pi = \Lambda + 2M, \qquad (5)$$

it is possible to write Q independently for P-waves and S-waves through the relaxation times, τ_ε^p and τ_ε^s (Robertsson et al., 1994). Hence, the relaxation function assumes the following definition:

$$\Pi = \pi \left[1 - \left(1 - \frac{\tau_\varepsilon^p}{\tau_\sigma} e^{-t/\tau_\sigma} \right) \right] H(t), \qquad (6)$$

and

$$M = \mu \left[1 - \left(1 - \frac{\tau_\varepsilon^s}{\tau_\sigma} e^{-t/\tau_\sigma} \right) \right] H(t), \qquad (7)$$

where is the relaxation modulus corresponding to S-waves and it is analogous to the shear modulus μ, Π is the relaxation modulus corresponding to P-waves and it is analogous to $\lambda + 2\mu$, where λ is the Lamé constant in the elastic case, τ_ε^p and τ_ε^s are the strain relaxation times for P and S-waves, respectively, and τ_σ, the stress relaxation time for both, P and S-waves.

The strain tensor ε_{kl} can be written in terms of the particle displacement vector u_i:

$$\varepsilon_{kl} = \frac{1}{2}(\partial_k u_l + \partial_l u_k). \qquad (8)$$

It gives then:

$$\begin{cases} \partial_j \sigma_{ij} - \rho \partial_t v_i = -\rho f_i \\ \dot{\sigma}_{ij} = (\dot{\Pi} - 2\dot{M}) * \partial_k v_k + 2\dot{M} * \partial_i v_j & (i = j) \\ \dot{\sigma}_{ij} = \dot{M} * (\partial_i v_j + \partial_j v_i) & (i \neq j) \end{cases} \qquad (9)$$

The use of the memory variables avoids the convolution calculation. They are obtained from the solution of the following differential equations:

$$\dot{r}_{ij} = -\frac{1}{\tau_\sigma} \left(r_{ij} + \left(\pi \left(\frac{\tau_\varepsilon^P}{\tau_\sigma} \right) - 2\mu \left(\frac{\tau_\varepsilon^S}{\tau_\sigma} \right) \right) \partial_k v_k + 2\mu \left(\frac{\tau_\varepsilon^S}{\tau_\sigma} \right) \partial_i v_j \right), \qquad (10)$$

for diagonal r_{ij} $(i = j)$, and

$$\dot{r}_{ij} = -\frac{1}{\tau_\sigma} \left(r_{ij} + \mu \left(\frac{\tau_\varepsilon^S}{\tau_\sigma} \right) (\partial_i v_j + \partial_j v_i) \right), \qquad (11)$$

for off-diagonal r_{ij} $(i \neq j)$.

Seismic Modelling

The first order stress-velocity viscoelastic wave equation presented (Eq. 9) is used to model synthetic seismograms. The staggered-grid Finite Difference (FD) solver has 2nd-order accuracy in time and 4th-order accuracy in space (Figure 2). The discretization applied to the equations follows the works from Virieux (1986), Levander (1988), Robertsson et al. (1994) and Moczo et al. (2018).

To avoid for spurious reflections at the limits of the computational domain, the absorbing boundary condition by Cerjan et al. (1985) is used. The amplitude of the seismic wave on each grid within the absorption area is decayed by the function

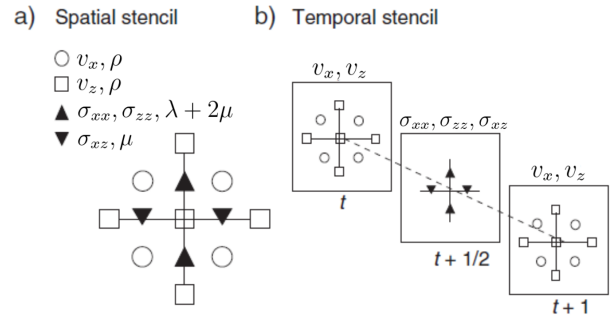$$G(i) = \exp \left[-\lambda^2 (n_0 - n)^2 \right], \ n = 0, 1, 2, ..., n_0, \qquad (12)$$

Figure 2: Staggered-grid FD configuration. (Modified from Schuster (2017)).

where λ is the attenuation coefficient, n is the grid index of the damping area, and n_0 is the layer number of the damping area (i.e. the index of the outermost layer) (Gao et al., 2017). Cerjan et al. (1985) use $n_0 = 20$ and $\lambda = 0.015$. In this work, the values set for these parameters were $n_0 = 100$ and $\lambda = 0.0025$.

The model has 1001 × 1001 grid points and the time step dt used is 0.35 ms. The grid spacing in the x and z directions is 3 m. A pressure source is located at 1503 m of offset and at 45 m of depth, which is a zero-phase Ricker with a central frequency of 40 Hz.

For comparison, an elastic modelling is also implemented. It can be simply obtained from the viscoelastic wave equations applying the limits $Q \to \infty$ and $\tau_\varepsilon / \tau_\sigma \to 1$.

Seismic data

The Búzios oil field is located in the central region of Santos Basin (see Figure 3), about 180 km from the coast of Rio de Janeiro, with water depth of 1940 m and area of 852.2 km². Its production started on April 2018 and, according to the bulletin from ANP (2019), it was responsible for 20% of hydrocarbons production of the brazilian pre-salt.
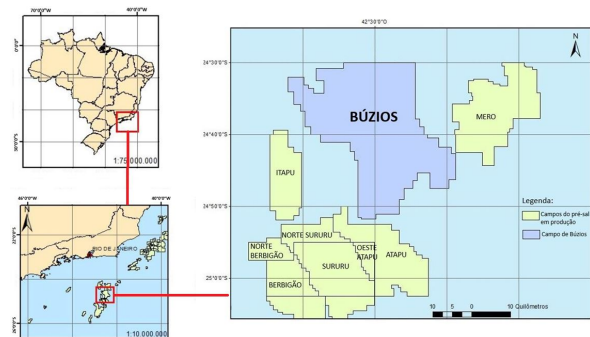

Figure 3: Location of Búzios oil field (Castro, 2019).

This work uses a near offset seismic data of the Búzios oil field with offset range from 147 to 158 m. The data also has low-cut filter, swell noise attenuation, debubble filter and resampling of 4 ms.

Results

In order to evaluate the seismic attenuation in the Búzios oil field, the comparison of the amplitude spectra is performed. Initially, three areas of the post-salt region in the seismic section are selected, as shown in Figure 4. The reason for choosing these regions is due to having nearly to plane parallel bedding. Each region has the same number of traces and interval time. In Figure 5, the amplitude spectra is extracted, where each color corresponds to the depth level.
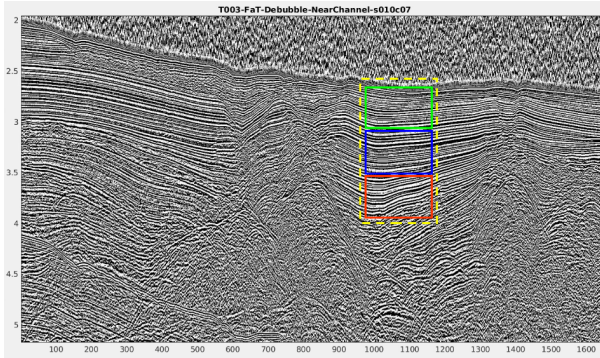

Figure 4: Near offset seismic data from Búzios field.

To seismic modelling, five tests are performed using geological model with four flat layered media, where the first layer is water. All physical properties of the geological model are presented in Table 1. In addition, to viscoelastic simulation, three sets of quality factor values, shown in Table 2, are used for configuration of layers 2 to 4 in four different arrangements. This strategy is used to reproduce the same seismic attenuation behaviour observed in real data. The central trace of pressure synthetic seismogram for each case is taken to extract the amplitude spectra in the seismic modelling.
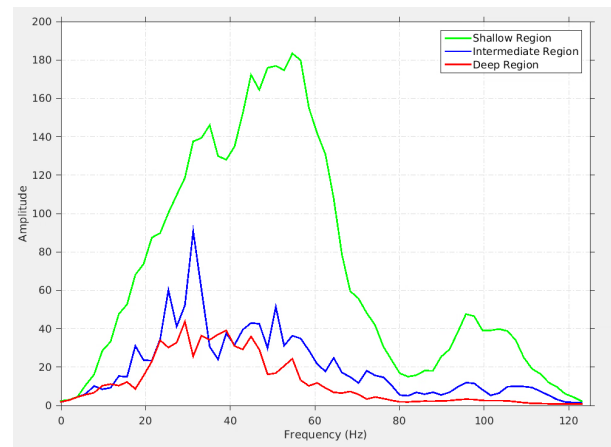
	v_p (m/s)	v_s (m/s)	ρ (kg/m^3)
Layer 1 (water)	1520	0	1050
Layer 2 (shallow)	2600	1600	2100
Layer 3 (intermediate)	3200	1960	2300
Layer 4 (deep)	4000	2260	2600

Table 1: Physical properties of the geologic model.
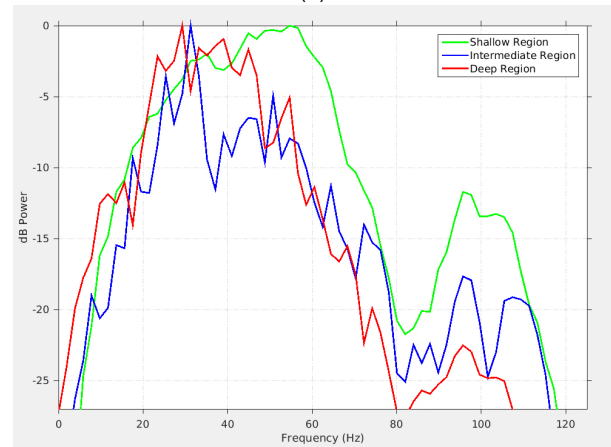
	Q_p	Q_s
Set 1	50	45
Set 2	90	70
Set 3	120	92

Table 2: Q values used in the viscoelastic modelling.

The elastic case is the first test performed as benchmark. In Figure 6, the amplitude spectra for the elastic case is shown. As expected, there is no difference among the spectra for the different layers, which shows the absence of attenuation and dispersion effects in the medium. This behavior does not match the seismic data. It confirms that an elastic modelling is not an adequate approach to describe the characteristics that affect seismic amplitude, phase and frequency content in the data of Búzios oil field.

(a)

(b)

Figure 5: (a) Amplitude and (b) dB Power spectra extracted from Búzios field seismic data in the selected regions (shown in Figure 4).
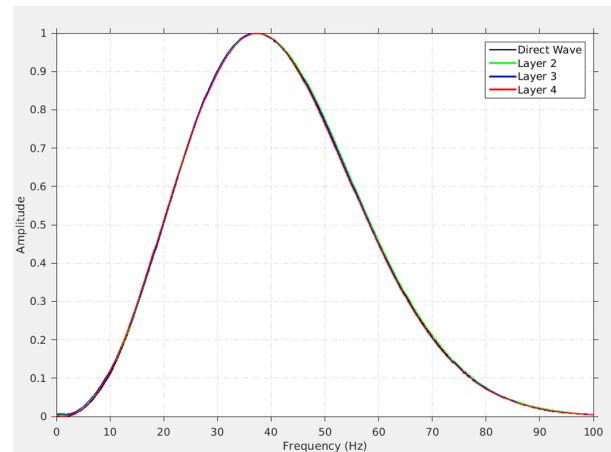

Figure 6: Amplitude spectra from the synthetic seismogram generated using the elastic model.

In the first viscoelastic case simulated, the highest attenuation (lowest Q values - set 1 in table 2) is placed in the intermediate layer. The shallow layer has the second highest attenuation (set 2) and the lowest (set 3) is in

the deep layer. The amplitude spectra obtained for this simulation is shown in Figure 7. As the first layer is water, there is no difference between the direct and reflected wave from the shallow layer (Layer 2). The separation between the blue and red spectra confirms that the intermediate layer yields greater attenuation effects on the subsequent layer than shallow layer on the intermediate. However, this behavior does match the seismic data (Figure 5).
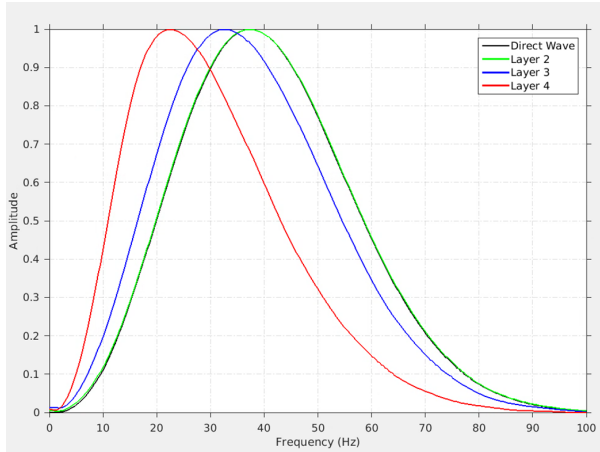

Figure 7: Amplitude spectra from synthetic seismogram generated using the viscoelastic modelling for setting 1. Colors distinguish the different layers: in green, the shallow, in blue, the intermediate and, in red, the deep.

In the second configuration simulated using the viscoelastic modelling, the layers are arranged from lowest to highest attenuation (Q values decreasing - sets 3, 2, 1). The amplitude spectra of the layers in this setting is shown in Figure 8. Because the most dissipative layer is placed on the deep layer, this test becomes the one with the lowest loss frequency content and, therefore, attenuation and dispersion than others. This configuration of quality factors also does not match the seismic data.
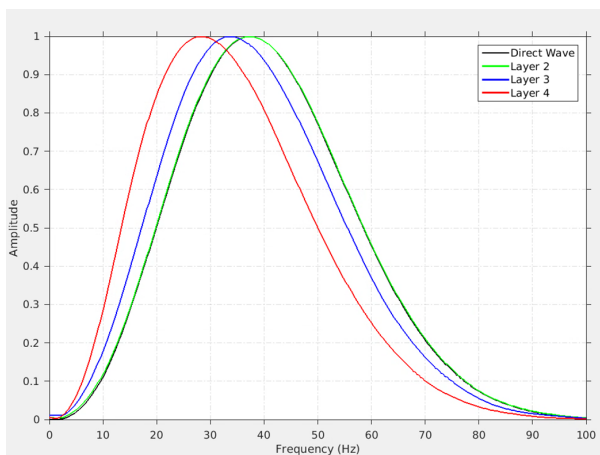

Figure 8: Amplitude spectra from synthetic seismogram generated using the viscoelastic modelling for setting 2. Colors distinguish the different layers: in green, the shallow, in blue, the intermediate and, in red, the deep.

The third viscoelastic simulation follows from the highest to lowest attenuating layer (Q values increasing - sets 1, 2,

3). The result of the amplitude spectra extracted for this case is presented in Figure 9. In this situation, there is a greater separation between the shallow layer (Layer 2) spectrum and the intermediate layer (Layer 3) spectrum than between intermediate layer spectrum and the deep layer (Layer 4) spectrum. This seismic attenuation behavior corresponds to that shown in Figure 5.
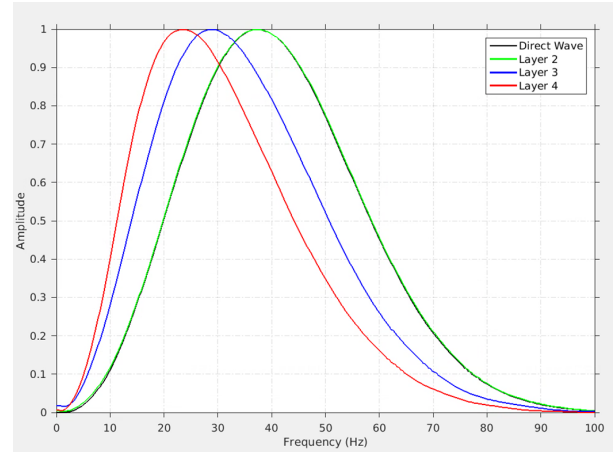

Figure 9: Amplitude spectra from synthetic seismogram generated using the viscoelastic modelling for setting 3. Colors distinguish the different layers: in green, the shallow, in blue, the intermediate and, in red, the deep.

Figure 10 shows the amplitude spectra of the fourth viscoelastic case simulated, which the shallow layer has the strongest attenuation (set 1, in Table 2) and the last ones have the same attenuation level (set 3, in Table 2). This configuration follows a similar trend to the previous test, where there is a greater spectra separation in the shallower layers. Nevertheless, the spectra separation between shallow layer and intermediate layer is quite greater when compared to the previous test. This is expected because the quality factor used for Layer 3 has slightly increased from 90 to 120. This result also does match the seismic data in the Búzios oil field.
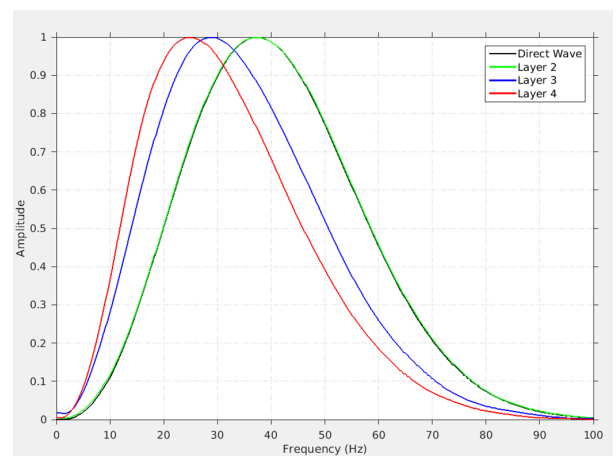

Figure 10: Amplitude spectra from synthetic seismogram generated using the viscoelastic modelling for setting 4. Colors distinguish the different layers: in green, the shallow, in blue, the intermediate and, in red, the deep.

The evaluation of the amplitude spectra from seismic data suggest that shallower sediments can contribute to a stronger attenuation than the deeper ones. Taking into account that attenuation is strongly affected by fluid saturation, pore fluid viscosity, confining pressure, pore geometry (Jones, 1986), thus slow formations in general must have a higher attenuation level. It is important to highlight that the amplitude spectra behavior only describe the attenuation in that region shown in Figure 4. Other regions should be investigated in order to map a more complete evaluation of the seismic attenuation in the Búzios oil field.

Conclusions

The SLS viscoelastic model simulates the behaviour of the amplitude spectrum from the seismic data of Búzios field around of the 40 Hz central frequency. The analysis of the amplitude spectra from the seismic data of the post-salt layer of the Búzios field and from the viscoelastic simulations allows us to obtain a qualitative relation of the Q factor distribution in the region under study. The similarity between the amplitude spectra from the seismic data and from the viscoelastic modelling with settings 3 and 4 indicates that the shallower sediment is more dissipative (has lower Q values) than the deepest ones.

Acknowledgments

References

ANP. Boletim da produção de petróleo e gás natural:, maio 2019.

Blanch, J. O., Robertsson, J. O. A., and Symes, W. W., Viscoelastic Finite Difference Modeling:, Technical Report 93-04, Department of Computational and Applied Mathematics, Rice University, 1993.

Carcione, J. M., 2015, Wave Fields in Real Media: Wave Propagation in Anisotropic, Anelastic, Porous and Electromagnetic Media: Elsevier, third edition.

Castro, T. M., 2019, Avaliação dos reservatórios carbonáticos do pré-sal no campo de búzios, bacia de santos: Dissertação de Mestrado, UFF.

Cerjan, C., Kosloff, D., Kosloff, R., and Reshef, M., 1985, A nonreflecting boundary condition for discrete acoustic and elastic wave equations: Geophysics, **50**, no. 4, 705–708.

Christensen, R. M., 1982, Theory of Viscoelasticity: An Introduction: Academic Press Inc.

Fan, N., Zhao, L. F., Xie, X. B., Ge, Z., and Yao, Z. X., 2016, Two-dimensional time-domain finite-difference modeling for viscoelastic seismic wave propagation: Geophysical Journal International, **206**, no. 3, 1539–1551.

Findley, W., Lai, J., and Onaran, K., 1989, Creep and relaxation of nonlinear viscoelastic materials: with an introduction to linear viscoelasticity: Dover Publications.

Gao, Y., Song, H., Zhang, J., and Yao, Z., 2017, Comparison of artificial absorbing boundaries for acoustic wave equation modelling: Exploration Geophysics, **48**, no. 1, 76–93.

Jones, T. D., 1986, Pore fluids and frequency-dependent wave propagation in rocks: Geophysics, **51**, no. 10, 1939–1953.

Levander, A., 1988, Fourth-order finite-difference P-SV seismograms: Geophysics, **53**, no. 1, 1425–1436.

Moczo, P., Kristek, J., and Galis, M., 2018, 3d finite-difference schemes: The Finite-Difference Modelling of Earthquake Motions, 166–198.

Poynting, J., and Thomson, J., 1903, Properties of matter: Nature, **67**, no. 1736.

Robertsson, J. O. A., Blanch, J. O., and Symes, W. W., 1994, Viscoelastic finite-difference modeling: Geophysics, **59**, no. 9, 1444–1456.

Schuster, G. T., 2017, Seismic Inversion: Society of Exploration Geophysicists.

Virieux, J., 1986, P-SV wave propagation in heterogeneous media: Velocity-stress finite-difference method: Geophysics, **51**, no. 4, 889–901.

Wang, Y., 2008, Seismic inverse Q filtering: Wiley.

Zener, C., 1948, Elasticity and anelasticity of metals: Univ. of Chicago Press, **3**.